Phenotypic plasticity stimulated by cooperation fosters pattern diversity of bacterial colonies

Dranreb Earl Juanico
Department of Mathematics, School of Science and Engineering, Ateneo de Manila University, Loyola Heights, Quezon City 1108, Philippines
(Received 15 March 2012; revised manuscript received 19 June 2012; published 23 July 2012)

Colonies of flagellated bacteria on agar plates are known to take on diverse morphologies. A diffusion-reaction model is proposed for bacterial-colony pattern formation on a surface due to time scale separation between the slow mass migration of bacteria from the point of inoculation, and the fast, but localized, dynamics of bacterial phenotypic plasticity stimulated by public-goods cooperation and phenotypic switching. By considering two switchable phenotypes in the population, the model generates pattern diversity typifying those reported by experimental studies.

DOI: 10.1103/PhysRevE.86.011920 PACS number(s): 87.18.Hf, 05.45.−a, 87.23.Cc

I. INTRODUCTION

Bacteria have survived the harshest environments on Earth through their uncanny ability to adapt. Striking illustrations of such adaptability are the diverse colony patterns they create (e.g., by *Bacillus subtilis*) [1,2]. On a flat agar plate, morphology ranges from the featureless disk to fringelike and branchy structures [3]. While previous models attempted to address how these patterns form, an explicit link between pattern diversity and the thrust for survival, especially the role of cooperation within that context [4–6], has yet to be made. A recent proposal suggests that bacterial survival in social settings rests on the plasticity between sedentary and nomadic lifestyles [7]. On one hand, bacteria might stay in cooperative consortia such as biofilms which offer protection against antibiotics, thus promoting population growth; on the other hand, they might retain high mobility to enhance the prospects of foraging [8]. However, each lifestyle also poses risks: the sedentary phenotype is vulnerable to competitive degradation due to overcrowding, and the nomadic phenotype is threatened by the higher chances of encountering antimicrobial substances. A mathematical model is hereby proposed to show how bacteria might capitalize on phenotypic plasticity in colony formation to adapt to conditions presented by their environment.

The evolution of bacterial colony on an agar plate is modeled by a diffusion-reaction system, wherein bacteria density grows and propagates in time within a Laplacian nutrient field. In this model, bacteria can take on two phenotypes, namely, *proliferator* and *migrator*. The two-phenotype picture is motivated by the typology devised in models of colony growth, e.g., swimmers and swarmers [9], and cooperators and defectors [6], and accords with the discovery of two developmental states of *B. subtilis* during mid-log growth phase [10]. Proliferators have low mobility compared to migrators, but migrators have a lower relative population growth rate than proliferators. Furthermore, since bacteria are known to exhibit phenotypic plasticity [11], the model allows for switching from one phenotype to another at a certain rate. Phenotypic switching is widely considered as a hedge tool that bacteria utilize to adapt to uncertain environments [11].

II. BACTERIAL-COLONY PATTERN FORMATION: MATHEMATICAL MODEL WITH BIOLOGICAL JUSTIFICATION

The following system is the proposed mathematical model that is able to generate five morphotypes discerned previously by experimental studies on colony pattern formation by *B. subtilis* [3,12]: DLF (diffusion-limited fractal); RE (rough edged); DBM (dense-branching morphology); CT (concentric terraces); and SD (spreading disk):

$$\partial_t x(\vec{r},t) = \nabla\cdot[D_x(\rho,x)\nabla x] + \beta\rho x - \left(\frac{x+y}{\kappa_x}\right)x + 4\left\{\frac{x\rho}{x+y} - \xi\rho\right\}x - \alpha x + \alpha y\,, \tag{1}$$

$$\partial_t y(\vec{r},t) = \nabla\cdot[D_y(\rho,x)\nabla y] + \beta\rho y - \left(\frac{x+y}{\kappa_y}\right)y + 4\left\{\frac{x\rho}{x+y}\right\}\tau y - \alpha y + \alpha x\,, \tag{2}$$

$$\partial_t n(\vec{r},t) = D_n\nabla^2 n - \mu(x+y)\rho\,. \tag{3}$$

While the above system [Eqs. (1)–(3)] is defined in the same spirit as known diffusion-reaction models of bacterial pattern formation (see Ref. [13] for a review), such types of models could not account for all patterns, especially the DLF and CT, without auxiliary stochasticity or assumptions of noise statistics (see for instance Ref. [2]). For the purpose of incorporating noise into the model, a coarse-grained approach is chosen for solving the system with consideration of the fact that the bacterial colony is not exactly a continuum field in the microscopic scale but rather one consisting of discrete bacterial cells.

The system is discretized and solved over a square grid of size L. A grid element (denoted "cell" hereinafter) at position $\vec{r}$ is described at any time t by local densities $x(\vec{r},t)$ and $y(\vec{r},t)$ of proliferators and migrators, respectively, and the nutrient level $n(\vec{r},t)$. The variable $\rho = n/(\tilde{n}+n)$ is based on the Michaelis-Menten kinetics for microbial growth by nutrient uptake [14]. By suitable rescaling, $\tilde{n} = 1$ is set without loss of generality [15]. Lastly, the parameter μ, which represents the per-capita rate of nutrient consumption, is fixed at 4 (per cell per Δt)

TABLE I. Rates in the model.

Rate	Value	Definition	Reference
β	$0.044\ \Delta t^{-1}$	Maximum specific birth rate	[16]
κ_x	0.125	Proliferator carrying capacity	[17]
κ_y	1.25	Migrator carrying capacity	
ξ	$0.2\ \Delta t^{-1}$	Cost of public-good production	
α	$0.0098\ \Delta t^{-1}$	High per-capita switching rate	[18]
	$0.12\ \Delta t^{-1}$	Low per-capita switching rate	

without loss of generality (i.e., its exact value has negligible influence on the results).

Table I presents a summary of the rates and constants, including carrying capacity (the inverse of which is a rate). In total, the model has two independent free parameters: initial nutrient level n_0, and τ, which serves as proxy for agar content, hence surface softness.

A. Time scale separation

The crucial assumption made in solving the diffusion-reaction system is the separation of time scales between macroscopic colony development (i.e., the incubation time it takes to produce a discernible colony pattern) and the microscopic population dynamics, arising from phenotypic plasticity, at length scales corresponding to Δr (about 200 μm). Experimental observations indicate that the fastest growing pattern (i.e., the SD) takes about half a day (12 h) to grow a diameter of about 5 cm [3]. On the other hand, microscopic imaging observations of the colony edge and interior indicate the presence of vortical flows which seem to facilitate bacteria mixing within time scales in the order of <1 s [19–21]. Mixing in turn is seen to facilitate bacterial interactions as it allows grouping and regrouping on the fast time scale. Furthermore, doubling time for bacteria is within 25–30 min in the case of *Bacillus subtilis* so that a considerable number of binary-fission events should have taken place within the chosen time unit Δt of 14 min. This leads us to the simplification that the diffusion and reaction parts in Eqs. (1)–(3) may be treated separately. Thus, each part may be solved in a modular manner using different approaches, and subsequently combined together to provide the full solution. In particular, the reaction parts are solved using a stochastic Gillespie method acting on population numbers X and Y converted from x and y, respectively (see Sec. III A), whereas the diffusion parts (assumed to have a slow effect on the pattern) are solved using finite-difference schemes acting on density values x and y (Sec. III B).

B. Boundary and initial conditions

Zero-flux boundary conditions apply to the nutrient field in Eq. (3) because nutrients are not replenished throughout the incubation period, in accordance with reported experiments [3,13]. Initially, nutrients are uniformly spread across the agar plate, and a bacteria inoculum is placed at the center of the plate. Motivated by experimental accounts, the inoculum is made up of vegetative colony-forming units (c.f.u.) for which the authors in Ref. [3] have outlined an experimental procedure. In standard procedures for inoculation, bacteria are first cultured in fermented nutrient broth and then brought out (and subsequently inoculated onto an agar plate) after they have reached a certain growth phase (i.e., middle to upper part of the log phase) [22]. In the log phase, bacteria are rapidly participating in binary fission (hence, vegetative), from which it is surmised that they are less flagellated on the basis of molecular mechanisms akin to the flagellation synthesis constraint seen among eukaryotes [23], through which fissioning cells synthesize less flagella [7]; hence, the inoculum is likely to be made up of mostly proliferators. Furthermore, the inoculation procedure aims to obtain an almost pure bacterial population of a certain phenotype [22]. Accounting for minor deviations from purity, the inoculum used in the simulations is set with a composition of $\geqslant 97\%$ proliferators, and placed at the center of the grid. Deducing from reported optical-density measurements of the inoculum [3], a $200 \times 200\ \mu\text{m}^2$ patch should contain about $B_0 = 8000$ bacteria. Lastly, nutrients are distributed uniformly across the grid at initial level n_0.

C. Motility mechanisms

The diffusion functions D_x and D_y describe the *en-masse* mobility of proliferator and migrator phenotype, respectively. These functions are motivated by two known classes of bacterial surface translocation, hereby referred to as *active* and *passive* motility [24,25]. Active motility is based on flagella and works best on a soft medium. On the other hand, passive motility (driven by outward population pressure) is facilitated, for instance, by surfactants secreted by bacteria themselves and is an adaptation used for translocation on harder surfaces. Thus, we define the following:

$$D_y(\rho,x) = \begin{cases} 4\rho & \text{for active motility,} \\ 0.125x & \text{for passive motility,} \end{cases} \tag{4}$$

$$D_x(\rho,x) = \gamma D_y\,, \tag{5}$$

wherein the factor $\gamma < 1$ denotes the slow relative mobility of proliferators. For simplicity, $\gamma = 0.2$ is fixed. While the factor 4 in Eq. (4) is arbitrarily chosen, it is motivated by previous experimental studies that estimate bacterial mobility around the same order of magnitude as nutrient diffusivity D_n on soft surfaces [3]. The proportionality with ρ is prompted by the energy requirement to drive flagella, which is supported by the observation of no (or minimal) bacterial movement at the colony interior where nutrient is depleted first. The factor 0.125 in Eq. (4) is arbitrarily set to emphasize that colony expansion powered by passive motility is much slower than nutrient diffusion. It is proportional to x because mobility is facilitated by proliferators secreting public goods, such as surfactant [3].

D. Background Fisher-type population dynamics

The rate $\beta\rho$ in Eqs. (1) and (2) represents specific birth rates. Since $\rho \leqslant 1$, β represents a maximum specific rate which has been estimated experimentally. In *B. cereus*, for example, $\beta \approx 0.19$ per hour [16]; so, in the model $\beta = 0.044$ (per unit time, $\Delta t = 14$ min).

In more precise terms, the densities x and y are converted into population numbers X and Y, respectively, whereby B_0

serves as a scaling factor (Sec. III C). The conversion is necessary in carrying out the stochastic Gillespie algorithm for solving the reaction kinetics part. Since $\Delta r = 1$, it follows that $x = X/B_0$ and $y = Y/B_0$. The nominal carrying capacity for migrators K_y is set at 10 000 (to the same order as $B_{\max}$) from which follows that $\kappa_y = K_y/B_0 = 1.25$. On the other hand, $K_x = 1000$ (an order lower) for proliferators so that $\kappa_x = 0.125$.

Combining rates of the form $\beta\rho - (x + y)/\kappa$ in the reaction part of Eqs. (1) and (2) reveals a logisticlike term. When further combined with a diffusion term, the right-hand sides of Eqs. (1) and (2) describe a Fisher-type diffusion-reaction system, which is commonly implemented in modeling bacteria-colony patterns [26].

E. Public-goods cooperation

The terms within $\{\cdots\}$ in Eqs. (1) and (2) represent per-capita rates due to public-goods cooperation [5,27]. The factor 4 denotes the strength of frequency-dependent selection arising from the said cooperation phenomenon. Proliferators invest a portion of their energy reserves $\xi\rho$ into the public good within the cell they belong to. The contributions are then pooled (i.e., $x\rho$) and divided equally among all members of the cell; hence, a dividend of $x\rho/(x + y)$ is received by each. The maximum specific contribution ξ by an individual proliferator is $\xi \leqslant 0.2\,\Delta t^{-1}$, although simulation results reveal that even $\xi \geqslant 0.095\,\Delta t^{-1}$ does not significantly change the morphological diagram of generated patterns.

The presence of τ in Eq. (2) sets the current model apart from usual public-goods cooperation models wherein the advantage due to defection or cheating is apparent only in the population growth rates [6,27]. A tradeoff between proliferation and mobility is hypothesized vis-a-vis the flagellation synthesis constraint seen in eukaryotes [23]. For migrators, the dividend is used primarily to maintain their higher relative mobility by means of flagella at the expense of proliferation. This explains why $\tau < 1$ in Eq. (2). In the model, τ is linked with mobility by way of the factor γ in Eq. (5), i.e., $\tau < 1 \Rightarrow \gamma < 1$, which expresses the tradeoff above hypothesized. However, no assumptions are made about the function $\tau(\gamma)$ since further biological observations are needed to specify such function.

The above formulation for the public-goods cooperation is also in agreement with a recent generalization to Hamilton's rule applied to microbial cooperation [5]. The generalized Hamilton's rule allows for variation in the benefits received, in terms of increased lifetime reproduction, depending on the individual type. Furthermore, it eliminates the assumption of additivity, thus allowing for strong selection effects typical of microbial populations [5].

F. Phenotypic switching

The coupling terms involving α in Eqs. (1) and (2) are motivated by findings that isogenic bacteria undergo a process known as *phenotypic switching*, which leads to diversification [11]. Such a process has also been known to control surface motility in *B. subtilis* through the action of certain genes involved in the biosynthesis of surfactin (a lipoprotein) and flagella [28]. Estimates on rates from previous studies suggest that there is a directional bias in the rates (i.e., faster in one direction compared to the other) [29–31]. But, for simplicity the model assumes that phenotypic switching is direction invariant. The per capita switching rate α is within the realm of high-frequency variation, in the order of between 10^{-3} and 10^{-2} per generation [30,32]. Assuming a generation time between 26–65 min (in the case of *B. subtilis* incubated at 37 °C [33]), it is considered in the model that $\alpha = 0.0098\,\Delta t^{-1}$ for low-rate phenotypic switching, based from experimental estimates [18]. A high rate is also considered with $\alpha = 0.12\,\Delta t^{-1}$.

Furthermore, the per capita switching rate α is generally constrained to be a function of the initial nutrient level n_0; particularly, $\alpha(n_0) > 0$ is a decreasing function with n_0, which is motivated by the finding that increasing stress conditions (associated with decrease in n_0, for example) speeds up switching rates [34].

III. NUMERICAL METHODS

The diffusion-reaction system is solved by treating separately the diffusion and reaction parts, and then combining the results to move the solution a time step forward. The diffusion part describes the macroscopic, continuum, but rather slow, dynamics of colony expansion (time scale of at least 12 h [3]). On the other hand, the reaction kinetics reflects the rapid reorganization of local populations (in terms of phenotypic composition) in all cells within the scale of 14 min.

A. Gillespie method: Reaction substep

Rather than solving the reaction kinetics deterministically, a stochastic Gillespie method is employed in a similar manner detailed in Ref. [35]. The motivation for this is that bacteria colonies are truly described as a population of discrete entities rather than as a continuum field. Each reaction rate is converted into a so-called *propensity*, which is a probability per unit time that the corresponding process takes place at all. By letting $X = X(\vec{r},t)$ and $Y = Y(\vec{r},t)$ be the number of proliferators and migrators, respectively, within cell at position $\vec{r}$ at time t, the propensities may be expressed in a straightforward manner for each reaction term. Furthermore, let B_0 denote the initial number of bacteria of the inoculum. From Eq. (1), the corresponding propensities are

$$a_0 = a_0[X \to X + 1] = \frac{\beta\rho}{4}X, \tag{6}$$

$$a_1 = a_1[X \to X - 1] = \left(\frac{X + Y}{4\kappa_x B_0}\right)X, \tag{7}$$

$$a_2 = a_2[X \to X + 1] = \left(\frac{\rho X}{X + Y}\right)X, \tag{8}$$

$$a_3 = a_3[X \to X - 1] = \xi\rho X, \tag{9}$$

$$a_4 = a_4[X \to Y] = \frac{\alpha}{4}X\,, \tag{10}$$

wherein the expression within $[\cdots]$ describes the process ("creation" or "annihilation" of a single individual of a certain phenotype) represented by a particular propensity. Similarly,

the propensities from Eq. (2) may be written as follows:

$$a_5 = a_5[Y \to Y + 1] = \frac{\beta\rho}{4} Y, \tag{11}$$

$$a_6 = a_6[Y \to Y - 1] = \left(\frac{X + Y}{4\kappa_y B_0}\right) Y, \tag{12}$$

$$a_7 = a_7[Y \to Y + 1] = \left(\frac{\rho X}{X + Y}\right) \tau Y, \tag{13}$$

$$a_8 = a_8[Y \to Y - 1] = 0, \tag{14}$$

$$a_9 = a_9[Y \to X] = \frac{\alpha}{4} Y. \tag{15}$$

Reactions are calculated starting at time $i = 0$ over a total time substep $\delta t = \Delta t/4$ as detailed further in Sec. III B, which also explains the factor $1/4$ in Eqs. (6), (7), (10)–(12), and (15).

Two random numbers, namely, φ_1 and φ_2, from a uniform distribution between 0 and 1 are drawn for the sake of determining the length of the time interval ε from one event to the next, and for deciding which reaction event occurs. By defining $A = \sum_{j=0}^{9} a_j$, ε is calculated as follows:

$$\varepsilon = -\ln(\varphi_1)/A.$$

To illustrate the basic scheme of the Gillespie algorithm, for example, the reaction represented by propensity a_3 is chosen if $(\sum_{j\leqslant 3} a_j)/A < \varphi_2 \leqslant a_3/A$. After the event takes place, time is updated such that $i \to i + \varepsilon$. Further reactions can still take place as long as $i < \delta t$.

B. Alternating direction implicit method: Diffusion substep

In order to solve the diffusion step, the operator-splitting scheme (also known as alternating-direction implicit, or ADI) is used whereby the time step is split into four parts that correspond to the four axes (up-down, left-right, and two diagonals) along which the finite spatial differences for the diffusion part are evaluated. Thus, given Δt, each substep δt corresponds to a time interval of only 3.5 min. For each δt, the order of evaluation with respect to axis is random. The ADI scheme used in this study is based on an isotropic finite-difference stencil proposed in Ref. [36].

C. Full solution at one time step Δt

A crucial step in the numerical method is the interconversion between density and population numbers. This is done by setting the size of a cell Δr to unity so that the cell area is also unity. The system [Eqs. (1)–(3)] is rescaled with respect to B_0. If x is density and X is the corresponding number, then $x = X/B_0$. Stochastic effects due to the finiteness of B_0 and the errors of interconversion from number to density and back seem to be less pronounced if B_0 is almost of the same order as the maximum capacity per cell $B_{\max}$. Another source of error with interconversion is the resolution limit $1/B_0$. If density x is below that limit, it will yield a zero count for X. But, as long as B_0 is large enough, the resolution limit should pose minimal numerical error.

For each δt, $x(t)$ and $y(t)$ for all cells are converted into numbers and put into the Gillespie algorithm (Sec. III A) to yield updated $X(t + \delta t)$ and $Y(t + \delta t)$ numbers, which are then converted back into updated densities: $x(t + \delta t)$ and $y(t + \delta t)$. Also updated is the nutrient level $n(t + \delta t)$. The diffusion step is subsequently solved to yield even more updated x, y, and n for all cells. The same process is done in all the other substeps until the full Δt is used up, at which time the variables have been updated to their values $x(t + \Delta t)$, $y(t + \Delta t)$, and $n(t + \Delta t)$ for all $\vec{r}$.

D. Colony pattern visualization

In order to visualize the colony pattern, the density at each cell is calculated by counting all existing bacteria as well as all bacteria that died in that cell. This method is reasonable because when a bacterium dies within a cell, it remains in that cell; furthermore, it is in agreement with colony patterns photographed in experimental observations [3].

IV. RESULTS

Figure 1 presents morphological diagrams for patterns generated by the model, and is plotted with respect to the control parameters n_0 and τ. Patterns are distinguished by visual inspection. Regimes of a particular pattern are recognized and are denoted as "phases." Figure 1 (A) corresponds to a bacteria population exhibiting active motility and for which phenotypic switching takes place at low rate (see Table I). On the left side of the diagram are phases characterized by high-density uniform disks dominated by proliferators, whereas on the right side is the low-density SD phase dominated by migrators [3]. Increasing τ from left to right corresponds to a change in the outcome of the public-goods game from proliferator dominance to prisoner's dilemma. The intermediate phases A2 and A3 feature an alternation of dominance between phenotypes. Phase A3 corresponds to the CT with its characteristic terraces, whereas A2 appears like the DBM with its dense branches at the interior.

Figure 1(B) is a diagram of patterns generated by imposing active motility but at high switching rate α. The primary effect of higher α is to make the DBM branches prominent (B2), and the CT terraces narrower (B3), compared to those shown in Fig. 1(A). Phase B1 is similar to A1, whereas B4 resembles a rosette rather than a uniform SD pattern as in A4. The "bright spots" on B4 patterns are due to the sporadic presence of proliferators induced by migrators switching into proliferators at higher rates.

Figure 1(C) illustrates the patterns generated by imposing only passive motility at low phenotypic switching rate. The left side of the diagram consists of patterns which expand much slower ($\sim 10^3\ \Delta t$) compared to phases in Figs. 1(A) and 1(B) ($\sim 10^2\ \Delta t$), whereas the right side is a no-growth phase (C4). Phase C2 corresponds to the DLF with its self-similar branches, the fractal dimension of which is estimated at $d_f = 1.72$ using the box-counting method, and is within the range of experimental estimates [37]. Phase C1 is an RE, the edge roughness of which is quantified by a Hurst exponent $H = 0.78$, which is in agreement with known estimates on *B. subtilis* colonies [38]. Phase C3 is characterized by dense branches and a rough edge, similar to that reported in Ref. [39], within the same region of parameter space.

Salient phase boundaries are analytically accounted for. The C1–C2 boundary may be accounted for by the Mullins-Sekerka instability of the colony front, which is present in C1 but not in

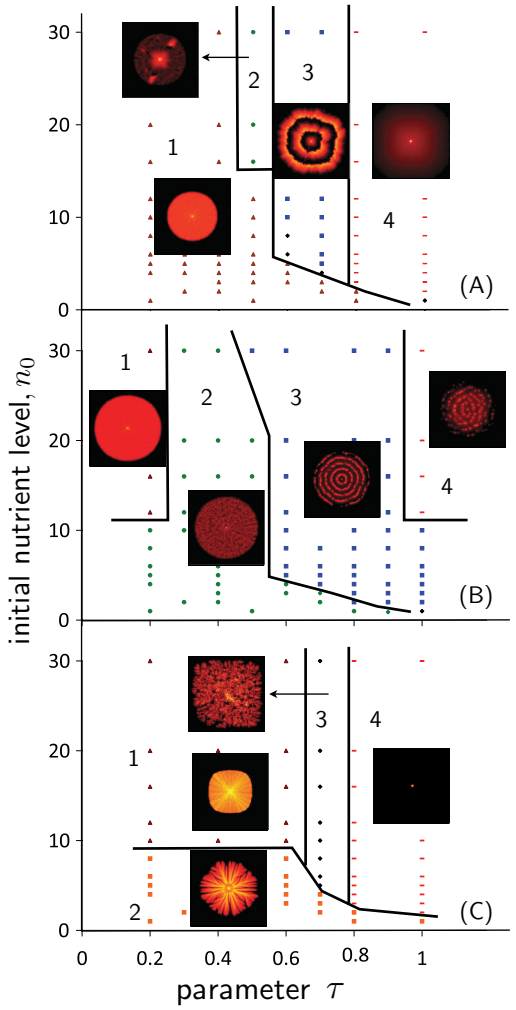

FIG. 1. (Color online) Morphological diagrams. Data points represent samples of different pairs of initial nutrient level n_0 and of "substrate softness" parameter τ. Distinct pattern regimes ("phase") deduced by inspection are labeled by numbers, wherein lines serve as guides that delineate phase boundaries. Representative patterns are shown for each phase. (A) active motility, low per capita phenotypic switching rate $\alpha = 0.0098\,\Delta t^{-1}$; (B) active motility, high $\alpha = 0.12\,\Delta t^{-1}$; and (C) passive motility, $\alpha = 0.0098\,\Delta t^{-1}$. Phase boundaries A3–A4 and C3–C4 denote the onset of migrator dominance at low α, whereas the phase boundary C1–C2 for $\tau \leqslant 0.6$ is an outcome of a Mullins-Sekerka front instability. Recognized patterns: A3, B3 (CT); A4 (SD); B2 (DBM); C1 (RE); C2 (DLF). A composite diagram A3 + A4 + B2 (bottom) + C1 + C2 approximates experimental morphological diagrams reported previously [3].

C2. A perturbation analysis reveals a dispersion relation $\omega(q)$, which states the growth rate ω of a particular perturbation mode of wave number q along the front. Two extreme cases are analyzed: $n_0 \ll 1$ and $n_0 \gg 1$. In the former case, $\omega(q) > 0$, $\forall q > 0$, whereas in the latter case, $\omega(q) < 0$, $\forall q > 0$.

A simplified analysis of the traveling colony front is carried out through a rescaled form of Eq. (3):

$$\partial_t n = \nabla^2 n - \mu b \frac{n}{n+1}\,, \tag{16}$$

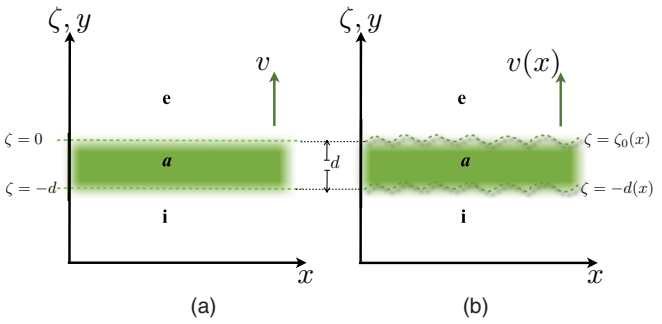

FIG. 2. (Color online) Sketch of the plane-wave sharp interface in the comoving frame (ζ,x), where $\zeta = y - vt$ with v being the front velocity. The regions are designated as **e** (external uncolonized area), **a** (active region), and **i** (inactive region). (a) Unperturbed plane wave: $\zeta = 0$ is designated as the front, whereas the tail is behind it at $\zeta = -d$; (b) perturbed plane wave: $\zeta_0(x) = \delta \cos qx$ and $d(x) = d - \delta \cos qx$; the velocity of the front is now designated as a function of x.

where $b = x + y$ denotes the total bacterial density at the front, which is approximately constant as the colony expands outward. Equation (16) may be written into an approximate form for $n_0 \gg 1$ as

$$\partial_t n \approx \nabla^2 n - K\,, \tag{17}$$

where K is a constant denoting the fixed consumption rate at the front by a constant density of bacteria, and since $n/(n+1) \to 1$ at the front for large n_0. On the other hand, for small n_0, Eq. (16) may be written into an approximate form as

$$\partial_t n \approx \nabla^2 n - kn\,, \tag{18}$$

where k is a fixed consumption rate per nutrient owing to $n/(n+1) \approx n$ at the front for small n_0. Equations (17) and (18) are solved by treating front propagation as a sharp interface problem (see Fig. 2). A comoving axis is defined by assigning a variable

$$\zeta = y - vt\,,$$

which moves with the front at velocity v. The plane wave is perturbed by an oscillatory function

$$\delta(x) = \delta \cos qx\,,$$

whose amplitude $\delta \ll 1$ and wherein q denotes the wave number of that perturbation.

The goal is to determine a dispersion equation of the form

$$\omega(q) = \frac{\dot{\delta}}{\delta},$$

which relates the growth rate of amplitude to the wave number q of the perturbation. If $\omega(q = a) > 0$, then the mode with wave number a grows in time; on the other hand, if $\omega(a) < 0$, then the a mode decays in time.

In the large-n_0 case, perturbation of the interface leads to the following solution:

$$n[\zeta + \delta(x)] = n^0(\zeta) + n^1(\zeta)\delta(x) = n^0 + n^1 \delta \cos qx\,. \tag{19}$$

Based on the proposed solution [Eq. (19)] and the definition for ζ, Eq. (17) may be rewritten in one-dimensional form

(neglecting explicit dependence with time t) as follows:

$$\begin{aligned}\frac{\partial^2 n^0}{\partial\zeta^2}+v\frac{\partial n^0}{\partial\zeta}-K\Theta=0,\\ \frac{\partial^2 n^1}{\partial\zeta^2}+v\frac{\partial n^1}{\partial\zeta}-q^2 n^1=0\,,\end{aligned} \tag{20}$$

where $\Theta=1$ in region **a** in which nutrient is actively consumed, and $\Theta=0$ in regions **e** and **i** (see Fig. 2).

A particular solution to Eq. (20) is found by introducing the following boundary and asymptotic conditions:

$$\lim_{\zeta\to\infty} n_e(\zeta)=n_0, \tag{21}$$

$$n_e[\zeta_0(x)]=n_a[\zeta_0(x)], \tag{22}$$

$$\partial_\zeta n_e[\zeta_0(x)]=\partial_\zeta n_a[\zeta_0(x)], \tag{23}$$

$$n_a[-d(x)]=n_i[-d(x)]=\lambda n_0, \tag{24}$$

$$\partial_\zeta n_a[-d(x)]=\partial_\zeta n_a[-d(x)], \tag{25}$$

$$\lim_{\zeta\to-\infty} n_i(\zeta)=\lambda n_0\,, \tag{26}$$

wherein $\zeta_0(x)=\delta\cos qx$ and $d(x)=d-\delta\cos qx$. The factor $\lambda<1$ denotes the fraction of the initial nutrient level n_0 left unconsumed at the inactive region. The general forms of the solutions for each region are as follows:

$$\begin{aligned}n_e(\zeta,x)&=A_e^0-B_e^0\frac{e^{-v\zeta}}{v}+\left\{A_e^1e^{-\widehat{\alpha}\zeta}+B_e^1e^{-\widehat{\beta}\zeta}\right\}\delta\cos qx,\\ n_a(\zeta,x)&=\frac{K\zeta}{v}+A_a^0-B_a^0\frac{e^{-v\zeta}}{v}+A_a^1e^{-\widehat{\alpha}\zeta}\delta\cos qx,\\ n_i(\zeta,x)&=A_i^0-B_i^0\frac{e^{-v\zeta}}{v}+\left\{A_i^1e^{-\widehat{\alpha}\zeta}+B_i^1e^{-\widehat{\beta}\zeta}\right\}\delta\cos qx\,,\end{aligned}$$

where the A's and B's are coefficients to be determined, and $\widehat{\alpha}=(v+\sqrt{v^2+4q^2})/2$ and $\widehat{\beta}=(v-\sqrt{v^2+4q^2})/2$.

The coefficients are solved by applying the boundary conditions into Eq. (20), and truncating the resulting terms up to first order in δ. The important aspect is the perturbed solution $n_a(\zeta,x)$ for the active region, which is essentially the interface itself. Thus,

$$A_a^0=n_0-\frac{K}{v^2},\quad B_a^0=-\frac{K}{v}e^{-vd},\quad A_a^1=\frac{K}{v}e^{-\widehat{\alpha}d}\,.$$

Because the interface propagates due to passive-type motility, which is density dependent and rather slow, it is reasonable to assume that $v\ll 1$. This is confirmed by the large amount of incubation time required to see RE and DLF patterns exhibiting that type of motility. Thus, a further approximation is made such that

$$\widehat{\alpha}\approx|q|\,,$$

so that the perturbed solution for the active region is now (up to first order in v and δ) as follows:

$$\begin{aligned}n_a(\zeta,x)\approx n_0-\frac{K}{v^2}(1-e^{-v(\zeta+d)})+\frac{K\zeta}{v}\\ +\frac{K}{v}e^{-|q|(\zeta+d)}\delta\cos qx\,.\end{aligned} \tag{27}$$

Furthermore, the interface width d is determined from the condition stated by Eq. (24):

$$d=\frac{(1-\lambda)vn_0}{K}\,. \tag{28}$$

The perturbation analysis by Gerlee and Anderson [40] proposed an identity related to the normal velocity of the propagating front:

$$\frac{\partial^2\zeta_0}{\partial t\,\partial x}=\left.\frac{\partial^2 n_a}{\partial\zeta\,\partial x}\right|_{\zeta=\zeta_0}, \tag{29}$$

which by virtue of Eqs. (27) and (28) yields the following dispersion equation:

$$\omega(q)=\frac{\dot{\delta}}{\delta}=-\left[\frac{K^2}{(1-\lambda)v^2}\right]\frac{|q|d}{n_0}e^{-|q|d}\,. \tag{30}$$

Equation (30) tells us that the growth rate $\omega<0$ for all wave numbers, which implies that any perturbation dies out eventually as the front propagates outward.

On the other hand, for the small-n_0 case, the governing equation (18) now takes on the dimensionally reduced form

$$\begin{aligned}\frac{\partial^2 n^0}{\partial\zeta^2}+v\frac{\partial n^0}{\partial\zeta}-k\Theta n^0=0,\\ \frac{\partial^2 n^1}{\partial\zeta^2}+v\frac{\partial n^1}{\partial\zeta}-(k\Theta+q^2)n^1=0\,,\end{aligned} \tag{31}$$

wherein Θ is defined as before. Consequently, the general form of the solution is the same for regions **e** and **i** as in the previous case. But, now the general solution for the active region **a** now takes on the following form:

$$n_a(\zeta,x)=A_a^0e^{-\widehat{\sigma}\zeta}+B_a^0e^{-\widehat{\tau}\zeta}+A_a^1e^{-\widehat{\varphi}\zeta}\delta\cos qx\,,$$

wherein $\widehat{\sigma}=(v+\sqrt{v^2+4k})/2$, $\widehat{\tau}=(v-\sqrt{v^2+4k})/2$, and $\widehat{\varphi}=(v+\sqrt{v^2+4k+4q^2})/2$. By applying the boundary conditions onto Eq. (31) and by considering $v\ll 1$, the following coefficients are determined up to first order in v:

$$\begin{aligned}A_a^0&=\frac{1+e^{-2d\sqrt{k}}}{2\sinh(2d\sqrt{k})}\frac{vn_0}{\sqrt{k}}+\mathcal{O}(v^2),\\ B_a^0&=\frac{1+e^{2d\sqrt{k}}}{2\sinh(2d\sqrt{k})}\frac{vn_0}{\sqrt{k}}+\mathcal{O}(v^2),\\ A_a^1&=-\frac{\sqrt{k}vn_0e^{-d\sqrt{k}}}{|q|+\sqrt{k+q^2}}(1+\coth(d\sqrt{k}))+\mathcal{O}(v^2).\end{aligned} \tag{32}$$

Furthermore, the interface width d is determined from the condition stated by Eq. (24):

$$d=\frac{1}{\sqrt{k}}\sinh^{-1}\left(\frac{v}{\lambda\sqrt{k}}\right). \tag{33}$$

By applying the identity in Eq. (29) into the perturbed solution $n_a(\zeta,x)$, and by considering further that $v\ll 1$, the dispersion equation is determined as

$$\omega(q)=-\sqrt{k+q^2}A_a^1(q)\,, \tag{34}$$

along with Eqs. (32) and (33). It turns out that $\omega>0$ for all q, but is a decreasing function of q.

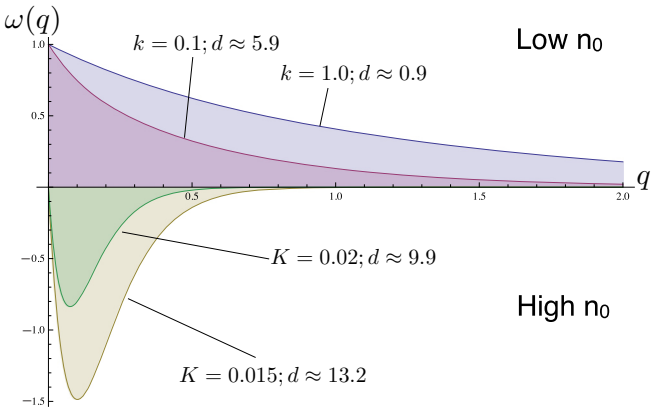

FIG. 3. (Color online) Dispersion equation $\omega(q)$ for two extreme cases of nutrient level n_0. The plots are derived by setting $v = \lambda = 0.01$. For the high-n_0 case, the plots are generated using Eq. (30), and d is calculated through Eq. (28) with $n_0 = 20$. For the low-n_0 case, the plots are generated from Eq. (34), and d is calculated through Eq. (33).

Superimposing plots based on Eq. (34) with those based on Eq. (30) presents us with a qualitative comparison of the front instability for large n_0 and small n_0. Figure 3 presents that comparison. The growth rate $\omega(q) > 0, \forall q$ for the low-n_0 case, which means that short-wavelength perturbations are amplified in time as the front propagates outward. This is consistent with the branched morphology of the DLF, which is observed at low n_0 in the simulations. On the other hand, $\omega(q) < 0, \forall q > 0$ for the high-n_0 case, which means that perturbations with nonzero wave numbers decay in time, thereby resulting in a more stable front without gaps. This is consistent with the RE observed at high n_0.

There should exist a crossover of the behavior of $\omega(q)$ with respect to q from low to high n_0 if the full nonlinearity of the original governing equation [i.e., the nonlinear dependence with n in Eq. (16)] is accounted for. Thus, it is shown that the Mullins-Sekerka instability is influenced by the initial nutrient level.

What the above analysis means is that for low n_0, the front is unstable to spatial perturbations so that gaps form along the front, exactly the mechanism known to generate branches of the DLF [3]. On the other hand, for high n_0, spatial perturbations along the front decay as the front propagates outward resulting in a stable front. Hence, the RE in phase C2 has a compact interior. A video animation compares the evolution of DLF and RE according to the said mechanism [41].

Finally, the A3–A4 and C3–C4 boundaries denote the value of τ above which migrators dominate the front. For low α such that the effect of phenotypic switching is approximately 0, it can be shown that the per capita reaction rates $\mathcal{R}_x$ and $\mathcal{R}_y$ in Eqs. (1) and (2), respectively, obey $\mathcal{R}_x < \mathcal{R}_y$ for $\tau > 1 - \xi$.

At the front, it is assumed that n_0 is high enough so that one can make the approximation $\rho \approx 1$. Furthermore, based on simulations, one may reasonably consider that $x, y \to 0$ at the front (i.e., bacteria density is too thin as it propagates outward). The inequality $\mathcal{R}_x < \mathcal{R}_y$ implies that the migrator phenotype dominates the front. That inequality, along with the aforementioned assumptions, leads to the following

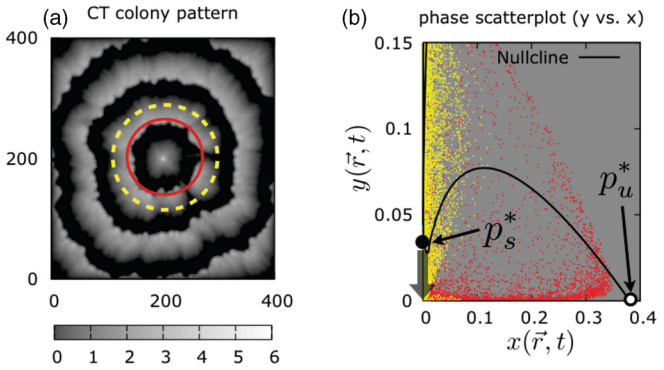

FIG. 4. (Color online) (a) CT by active motility ($n_0 = 16$, $\tau = 0.6$; $\gamma = 0.2$; $\alpha = 0.0098$; $\xi = 0.2$; time $= 600\Delta t \approx 5.8$ days). Circles indicate different times: *solid* ($t_1 = 150\Delta t$) corresponds to an onset of terrace formation; *dashed* ($t_2 = 252\Delta t$) to onset of rapid mass migration. (b) Phase scatterplot (migrator density y vs proliferator density x) snapshots at t_1 (*dark dots*) and t_2 (*bright dots*). Nullclines are shown as black curves. The hollow circle is the unstable equilibrium p_u^*, and the solid circle is the stable equilibrium p_s^*. Wide gray arrow pointing toward (0,0) indicates the effect of migration that induces a flow to the right and closer to p_u^*, which repels the trajectory and pushes it toward p_s^*. A migration-induced cycle thus generates the CT structure. The nonlinear mechanism is animated in video format [41].

condition:

$$\tau > \lim_{x,y\to 0}\left[1 - \xi\frac{x+y}{x} - \left(\kappa_x^{-1} - \kappa_y^{-1}\right)\frac{(x+y)^2}{4x}\right]. \quad (35)$$

Equation (35) is simplified by taking the constitutive relation $x = x(y) = \chi y$, where χ is a proportionality constant. This relation simply states that the density x of proliferators at the front is determined by proportion to the density y of migrators at the front, which is reasonable by considering that phenotypic switching gives rise to a certain proportion of one phenotype as a result of the presence of the other phenotype. Thus, Eq. (35) is simplified by evaluating the limit along the path in phase space for which $x(t)$ and $y(t)$ move together in the same direction. Hence, only the limit as $y \to 0$ is taken:

$$\tau > \lim_{y\to 0}\left[1 - (1+\chi)\xi - \left(\kappa_x^{-1} - \kappa_y^{-1}\right)(1+\chi)^2 y/4\right],$$

which simply gives

$$\tau > 1 - (1+\chi)\xi\,. \quad (36)$$

By considering that α is small, the amount of proliferators switching from migrators is expected to be small so that $\chi \ll 1$. Hence, Eq. (36) further simplifies into $\tau > 1 - \xi$, which for $\xi = 0.2$ gives the transitional value of τ to be $\tau^* = 0.8$.

As a matter of perspective, the condition $\mathcal{R}_x < \mathcal{R}_y$ implies migrator dominance in a prisoner's dilemma sense [6], which explains the low-density, migrator-dominated SD in phase A4 as well as the no-growth phase C4. As passive motility is defined in Eq. (4) is proportional to proliferator (public-good producing) density x, and since low α precludes migrators from switching into proliferators, the resulting low x at the front inhibits colony expansion for C4.

Finally, the CT [Fig. 4(a)] is rather curious because of its fringelike appearance. CT is also by far the most non-trivial of patterns formed by bacterial colonies because it does not

seem to fit into the notion of continuous outward propagation by a growing colony.

A linear stability analysis is carried out on Eqs. (1) and (2) at the colony front, where $\rho \approx n_0/(1+n_0)$, to elucidate the nonlinear mechanism behind CT structure. Assuming $\alpha \ll 1$, three fixed points are revealed, two of which are within the domain $x, y \geqslant 0$, namely, stable $p_s^* = (0, \{\beta\rho - \alpha\}\kappa_y)$ and unstable $p_u^* = [\{(4+\beta-\xi)\rho - \alpha\}\kappa_x, 0]$. A phase scatter plot in Fig. 4(b) demonstrates the dynamics leading to terrace formation. The trajectories are repelled by p_u^*, which implies that a front of proliferators are eventually taken over by migrators in prisoners-dilemma-like fashion [6]. The dynamics converges toward p_s^* (an absorbing state). However, the ensuing rapid outward migration thins out the front density, forcing the dynamics toward (0,0), which is not a fixed point. Subsequently, the flow is pushed toward the right approaching p_u^* once more and thus creating a cycle. This explanation accords with the two-thresholds hypothesis on the formation of concentric patterns in colonies of *Proteus mirabilis* and *B. subtilis*, which asserts that the alternation between migration and terrace formation is triggered not by quorum sensing but by localized phenotypic density variations [3,42].

V. DISCUSSION

A two-scale diffusion-reaction model has been proposed to account for the pattern diversity of bacterial colonies. It explicitly considers that survival in bacterial colonies is a dilemma between sedentary (proliferation for population growth) and nomadic (migration for foraging) lifestyles [7]. It merges concepts and ideas from diffusion-reaction modeling and the evolutionary game theory of public-goods cooperation, which, to the best of my knowledge, has not been implemented in previous models. The approach in solving the model also avoids the necessity for assuming extraneous noise statistics because the fluctuations are incorporated naturally as an offshoot of the discreteness of bacterial colonies. Pattern diversity is widest in scope at low phenotypic switching rates. Incorporating additional adaptive mechanisms through which bacteria recognize surface softness and respond accordingly by shifting between active and passive motility (e.g., [43]) would further justify a composite morphological diagram based on Fig. 1 that accounts for all known colony patterns as has been reported previously [3].

In the hopes of understanding the workings of ever more complex biological systems, this study opens up a gateway through which evolutionary game theory can be tested in colony-forming bacterial populations that develop spatial structures. It also contributes an opportunity to validate our understanding of bacterial self-organization based on what is currently known in microbiology about how bacteria adapt to uncertain and fluctuating environmental conditions.

ACKNOWLEDGMENTS

This work was made possible by a postdoctoral fellowship from the Alexander von Humboldt Foundation. Discussions with E. Frey and M. Leisner of the Ludwig-Maximilians-University in Munich, Germany, are gratefully acknowledged.

[1] E. Ben-Jacob, I. Cohen, and H. Levine, Adv. Phys. **49**, 395 (2000).
[2] K. Kawasaki *et al.*, J. Theor. Biol. **188**, 177 (1997).
[3] M. Matsushita *et al.*, Biofilms **1**, 305 (2004).
[4] S. A. West *et al.*, Annu. Rev. Ecol. Evol. Syst. **38**, 53 (2007).
[5] J. Smith, J. D. Van Dyken, and P. C. Zee, Science **328**, 1700 (2010).
[6] A. Melbinger, J. Cremer, and E. Frey, Phys. Rev. Lett. **105**, 178101 (2010).
[7] R. Kolter and E. P. Greenberg, Nature (London) **441**, 300 (2006).
[8] B. J. Crespi, Trends Ecol. Evol. **16**, 178 (2001).
[9] S. E. Esipov and J. A. Shapiro, J. Math. Biol. **36**, 249 (1998).
[10] D. B. Kearns and R. Losick, Genes Dev. **19**, 3083 (2005).
[11] B. Hallet, Curr. Opin. Microbiol. **4**, 570 (2001).
[12] H. Fujikawa, Phys. A (Amsterdam) **189**, 15 (1992).
[13] I. Golding *et al.*, Phys. A (Amsterdam) **260**, 510 (1998).
[14] D. K. Button, Microbiol. Rev. **49**, 270 (1985).
[15] More precisely, putting $\tilde{n}/n$ in place of n preserves ρ and the form of Eqs. (1) and (2). The effect is only rescaling μ in Eq. (3) to $\mu/\tilde{n}$.
[16] J. W. T. Wimpenny, J. Gen. Microbiol. **114**, 483 (1979).
[17] V. Rossetti *et al.*, J. Theor. Biol. **262**, 23 (2010).
[18] B. B. Kaufmann *et al.*, PLoS Biol. **5**, e239 (2007).
[19] H. P. Zhang *et al.*, Europhys. Lett. **87**, 48011 (2009).
[20] E. B. Steager, C. Kim, and M. J. Kim, Phys. Fluids **20**, 073601 (2008).
[21] C. Dombrowski, L. Cisneros, S. Chatkaew, R. E. Goldstein, and J. O. Kessler, Phys. Rev. Lett. **93**, 098103 (2004).
[22] R. E. Lincoln, J. Biochem. Microbiol. Tech. Eng. **2**, 481 (1960).
[23] N. King, Dev. Cell **7**, 313 (2004).
[24] D. B. Kearns, Nat. Rev. Microbiol. **8**, 634 (2010).
[25] R. M. Harshey, Annu. Rev. Microbiol. **57**, 249 (2003).
[26] J. Wakita *et al.*, J. Phys. Soc. Jpn. **63**, 1205 (1994).
[27] J. Y. Wakano, M. A. Nowak, and C. Hauert, Proc. Natl. Acad. Sci. USA **106**, 7910 (2009).
[28] D. B. Kearns *et al.*, Mol. Microbiol. **52**, 357 (2004).
[29] M. S. Bergen, E. Voss, and D. R. Soll, J. Gen. Microbiol. **136**, 1925 (1990).
[30] N. J. Saunders, E. R. Moxon, and M. B. Gravenor, Microbiology (Reading, UK) **149**, 485 (2003).
[31] N. Q. Balaban *et al.*, Science **305**, 1622 (2004).
[32] R. Villemur and E. Déziel, in *The Dynamic Bacterial Genome*, edited by P. Mullany (Cambridge University Press, New York, 2005), pp. 277–322.
[33] Y. Sadaie and T. Kada, J. Bacteriol. **163**, 648 (1985).
[34] B. L. Grau, M. C. Henk, and G. S. Pettis, J. Bacteriol. **187**, 2519 (2005).
[35] J. Horowitz *et al.*, Appl. Environ. Microbiol. **76**, 230 (2010).

[36] A. Kumar, J. Comput. Phys. **201**, 109 (2004).
[37] T. Matsuyama and M. Matsushita, Appl. Environ. Microbiol. **58**, 1227 (1992).
[38] J. Wakita *et al*., J. Phys. Soc. Jpn. **66**, 67 (1997).
[39] M. Ohgiwari, M. Matsushita, and T. Matsuyama, J. Phys. Soc. Jpn. **61**, 816 (1992).
[40] P. Gerlee and A. R. A. Anderson, Phys. Rev. E **75**, 051911 (2007).
[41] See Supplemental Material at http://link.aps.org/supplemental/10.1103/PhysRevE.86.011920 for Movie 1.
[42] Y. Yamazaki *et al*., Phys. D (Amsterdam) **205**, 136 (2005).
[43] G. Wang and D. Or, Environ. Microbiol. **12**, 1363 (2010).